Many-body wavefunction approach to topological quantum magnets

Kota IDO

Graduate School of Sciences and Technology for Innovation, Yamaguchi University
Tokiwadai, Ube, Yamaguchi 755-8611

I. INTRODUCTION

Strongly correlated quantum materials have long attracted attention as a class of materials that not only are of fundamental scientific interest, exhibiting intriguing phenomena such as high-temperature superconductivity, quantum spin liquids, and topological transport, but also hold potential for applications in advanced technologies [1–17]. To search for novel candidate materials with new functionalities or high performance, it is important to elucidate the microscopic mechanisms underlying these phenomena. This requires accurate methods for analyzing quantum many-body problems. Therefore, the development of high-accuracy methods, and of software implementing such methods, is progressing rapidly worldwide.

The variational Monte Carlo (VMC) method is a numerical method for analyzing such quantum many-body systems [18]. As its name suggests, VMC optimizes a trial wavefunction parameterized by variational parameters based on the variational principle, and then evaluates the expectation values of physical quantities via Monte Carlo sampling using the optimized trial wavefunction. Starting from many-body problems in liquid helium [19, 20], VMC has been applied to a wide range of many-body systems, including quantum lattice models such as the Hubbard model [21–23]. Although VMC has long been used for ground-state analysis, in recent years it has also been extended to nonequilibrium states [24–27], finite-temperature states [28, 29], open quantum systems [30–33], and excitation spectra [34–38], and its scope of application continues to expand.

The enhanced flexibility of VMC has been driven by improvements in computational resources, development and extension of methods and algorithms, and refinement of trial wavefunctions. An example of a VMC trial wavefunction capable of treating strongly correlated quantum materials is the pair-product wavefunction equipped with many-body correlation factors [39–41]. By introducing a large number of variational parameters not only into the many-body correlation factors but also into the pair-product wavefunction, one can represent a variety of quantum states including unconventional superconducting states, quantum spin liquids, magnetic states, and correlated metals. Furthermore, one can systematically improve the accuracy by employing tensor-network or neural-network representations of many-body correlation factors, thereby enabling high-accuracy analyses [42, 43]. Indeed, this type of wavefunction has been applied to strongly correlated quantum materials such as cuprate high-temperature superconductors, iron-based superconductors, and molecular solids, and its usefulness has been demonstrated [44–50].

In this report, we present our recent VMC analyses of quantum many-body systems that exhibit topological states, using the pair-product wavefunction. In Sec. II, we summarize the methods we employed, namely the VMC method and the pair-product wavefunction. Section III presents the VMC results for a frustrated Kondo lattice model [51] and the Kitaev-Kondo model. Finally, we devote Sec. IV to a summary of the results and discuss future prospects related to this topic, including the implementation of developed methods into open source software.

II. METHOD

A. Variational Monte Carlo method

In VMC, the expectation value of an operator $\mathcal{A}$ is evaluated by Monte Carlo sampling using a trial wavefunction $|\psi_{\boldsymbol{\alpha}}\rangle$ parameterized by variational parameters $\boldsymbol{\alpha}$ as follows:

$$\begin{aligned}\langle\mathcal{A}\rangle &= \frac{\langle\psi_{\boldsymbol{\alpha}}|\mathcal{A}|\psi_{\boldsymbol{\alpha}}\rangle}{\langle\psi_{\boldsymbol{\alpha}}|\psi_{\boldsymbol{\alpha}}\rangle} \\ &= \sum_x \rho(x)A(x) \approx \frac{1}{N_{\mathrm{MC}}}\sum_{i=1}^{N_{\mathrm{MC}}} A(x_i), \quad (1)\end{aligned}$$

$$\rho(x) = \frac{|\langle x|\psi_{\boldsymbol{\alpha}}\rangle|^2}{\langle\psi_{\boldsymbol{\alpha}}|\psi_{\boldsymbol{\alpha}}\rangle}, \quad A(x) = \frac{\langle x|\mathcal{A}|\psi_{\boldsymbol{\alpha}}\rangle}{\langle x|\psi_{\boldsymbol{\alpha}}\rangle}. \quad (2)$$

Here, N_{MC} is the number of Monte Carlo samples, and $|x\rangle$ denotes a real-space configuration of electrons or spins. Since $\rho(x)$ satisfies $\sum_x \rho(x) = 1$ and $\rho(x) \geq 0$, it can be regarded as a probability distribution. Provided that the inner product between the trial wavefunction and a real-space configuration is evaluable, real-space samples can be generated according to the probability distribution $\rho(x)$ using a Monte Carlo method such as the Metropolis-Hastings algorithm [52, 53]. Since Monte Carlo sampling can be parallelized over multiple independent Markov chains, it can be performed efficiently on supercomputers.

When the operator $\mathcal{A}$ is a physical observable such as an order parameter or an equal-time correlation function, $\mathcal{A}|x\rangle$ can be expressed as a linear combination of real-space configurations. Thus, $A(x)$ can be computed if the overlap integrals between the trial wavefunction and real-space configurations are evaluable. On the other hand, dynamical correlation functions involve a resolvent operator and thus cannot be expressed straightforwardly in terms of real-space configurations. To compute excitation spectra such as the optical conductivity and dynamical structure factors, one has to utilize methods such as Fourier-transforming a physical quantity obtained by real-time evolution, and evaluating the Lehmann representation on the subspace spanned by trial excited states [34–38].

The variational parameters $\boldsymbol{\alpha}$ can be optimized efficiently by the stochastic reconfiguration (SR) method [54], which is essentially equivalent to the natural gradient method, an optimization method in the field of machine learning [55].

B. Pair-product wavefunction with correlation factors

The pair-product wavefunction with many-body correlation factors is a trial wavefunction that can be flexibly applied to a wide range of quantum many-body systems [39–41]. The form of the wavefunction is defined as

$$|\psi_{\boldsymbol{\alpha}}\rangle = \mathcal{P}\,|\phi\rangle\,. \quad (3)$$

Here, $\mathcal{P}$ denotes a many-body correlation factor, and $|\phi\rangle$ is the pair-product wavefunction represented as

$$|\phi\rangle = \left(\sum_{i,j}\sum_{\sigma_i,\sigma_j} f_{i\sigma_i j\sigma_j} c^\dagger_{i\sigma_i} c^\dagger_{j\sigma_j}\right)^{N/2} |0\rangle\,, \quad (4)$$

where N is the number of fermions, i and j are site indices, σ_i and σ_j are spin indices, and $c^\dagger_{i\sigma_i}$ is the creation operator with spin index σ_i at site i. The pairing amplitude $f_{i\sigma_i j\sigma_j}$ contained in the pair-product wavefunction is treated as a variational parameter. The many-body correlation factor $\mathcal{P}$ is often constructed as a product of several correlation factors. The most conventional one is the Gutzwiller-Jastrow correlation factor [56, 57]:

$$\mathcal{P} = \mathcal{P}_{\mathrm{G}}\mathcal{P}_{\mathrm{J}}, \quad (5)$$

$$\mathcal{P}_{\mathrm{G}} = \exp\left(g\sum_i n_{i\uparrow}n_{i\downarrow}\right), \quad (6)$$

$$\mathcal{P}_{\mathrm{J}} = \exp\left(\frac{1}{2}\sum_{i\neq j} v_{ij}n_i n_j\right). \quad (7)$$

Here, $n_{i\sigma} = c^\dagger_{i\sigma}c_{i\sigma}$, $n_i = n_{i\uparrow} + n_{i\downarrow}$, and g and v_{ij} are variational parameters. Although these

many-body correlation factors contain operators in their exponents, most of them are diagonal with respect to real-space configurations, so their inner products with real-space configurations are easily computed. The inner product between the pair-product wavefunction and a real-space configuration can also be evaluated using the Pfaffian, a standard operation in linear algebra on skew-symmetric matrices, by exploiting the fact that $f_{i\sigma_i j\sigma_j} - f_{j\sigma_j i\sigma_i}$ forms a skew-symmetric matrix as a consequence of the fermion anticommutation relations. The trial wavefunction described above can therefore be handled within the VMC method.

III. APPLICATION TO TOPOLOGICAL MAGNETS

A. Kondo lattice model on the triangular lattice

We first present the VMC study of a magnetic topological state that emerges in the Kondo lattice model on the triangular lattice [51]. The Kondo lattice model is defined as a model in which localized spins and conduction electrons are coupled through the Kondo coupling, as follows:

$$\mathcal{H}_{\text{Kondo}} = -t \sum_{\langle i,j\rangle,\sigma} \left(c^{\dagger}_{i\sigma \text{c}} c_{j\sigma \text{c}} + \text{h.c.} \right) + J \sum_{i} \boldsymbol{S}_{i\text{c}} \cdot \boldsymbol{S}_{i\text{s}}, \tag{8}$$

$$\boldsymbol{S}_{i\lambda} = \frac{1}{2} \sum_{\sigma,\sigma'} c^{\dagger}_{i\sigma\lambda} \boldsymbol{\sigma}_{\sigma\sigma'} c_{i\sigma'\lambda} \tag{9}$$

Here, λ is an index distinguishing the conduction electrons (c) and the localized spins (s), $c^{\dagger}_{i\sigma\lambda}/c_{i\sigma\lambda}$ are the fermion creation/annihilation operators with spin index σ at site i in λ layer, $\boldsymbol{S}_{i\lambda}$ is the spin operator at site i in λ layer, and $\boldsymbol{\sigma}$ denotes the Pauli matrices. The fermion operators $c^{\dagger}_{i\sigma\text{s}}/c_{i\sigma\text{s}}$ representing the localized spins are called Abrikosov fermions [58]. Note that the Hilbert space of the localized spins under the Abrikosov fermion representation is enlarged compared to the original one. The ground state in the physical Hilbert space can be obtained by applying the Gutzwiller projection to exclude unphysical states, i.e., double occupancy and vacancy of the Abrikosov fermions at each site. $\langle i,j\rangle$ denotes a pair of neighboring sites. In addition, t is the hopping amplitude of the conduction electrons, and J is the Kondo coupling [59]. The Kondo coupling in the Kondo lattice model gives rise to the Ruderman-Kittel-Kasuya-Yosida (RKKY) interaction [60–62], a long-range effective magnetic interaction, and to the formation of Kondo singlets between the conduction electrons and the localized spins. The competition between these two effects has been shown to realize various intriguing quantum states, such as nonmagnetic Kondo insulators, magnetic phases accompanied by charge order, and unconventional superconductivity [63–72].

The Kondo lattice model has long been regarded as a representative effective model for heavy-fermion systems [68–72], but in recent years it has also attracted attention as a platform on which topological states such as topological insulators emerge [73–81]. It has been proposed theoretically that topological states are realized when the localized spins form a noncoplanar magnetic structure [73], and it has been pointed out that such states are indeed realized in Kondo lattice models with geometrical frustration, as represented by the triangular lattice [74–77]. However, most of these studies treat the localized spins in the classical limit, and it has been unclear whether such topological states remain stable when the localized spins are treated as quantum spins.

Using the variational Monte Carlo method, we analyze the Kondo lattice model on the triangular lattice at quarter filling up to a system size of $L = 16$, where L is the linear dimension of the system [51]. Preparing various magnetic states as initial states of the trial wavefunction and optimizing them, we find that a state with a noncoplanar triple-Q magnetic structure is

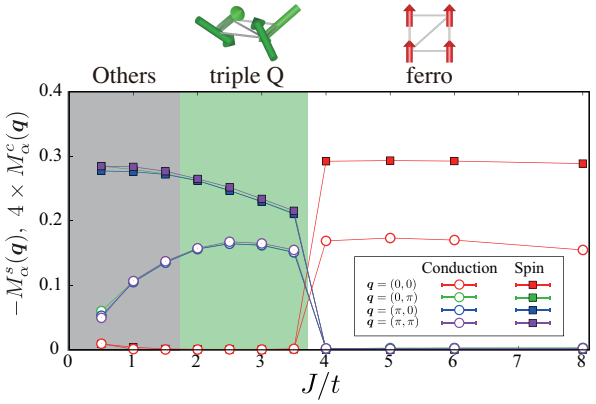

FIG. 1. J dependence of the magnetic order parameters of the localized spins and the conduction electrons for $L = 16$. Open and filled symbols represent the results for the conduction electrons and the localized spins, respectively. Shaded areas are guides to the eye for visualizing regions where the triple-Q state, the ferromagnetic state, and other magnetic states are stabilized. On top of the figure, the ground state in each region is labeled, and the schematic pictures of the spin configurations in the triple-Q state and the ferromagnetic state are also shown. Adapted from Ref. [51] with modifications for the present report.

most stable for $2 \lesssim J/t \lesssim 3.5$, a ferromagnetic state for $3.5 \lesssim J/t$, and other magnetic states for $J/t \lesssim 2$. Figure 1 shows the J dependence of the magnetic order parameters of the localized spins and the conduction electrons. The results for the ferromagnetic state are plotted where it is most stable, and those for the triple-Q state for the other values of J/t. We can see typical behavior in the Kondo lattice model: the formation of conduction-electron spin order due to the RKKY interaction, and the reduction of the localized spin moments due to Kondo screening. We also confirm that the triple-Q state is an insulator from the doping dependence of the chemical potential.

Previous studies in the classical limit have shown that the noncoplanar triple-Q magnetic insulator is a Chern insulator [76, 77], which is a type of topological insulator characterized by a nonzero Chern number. Because the triple-Q state we obtain is represented by the many-body wavefunction defined by Eq. (3), which goes beyond a mean-field treatment, it is desirable to directly compute a many-body topological number to determine whether it is a topological insulator or not. To address this, we extend to the VMC method a numerical approach for computing the many-body Chern number C using the twist operator [82, 83]. In previous studies, it has been pointed out that, by introducing a flux θ_x into the hopping terms along the x direction, the slope, with respect to the flux θ_x, of the argument of the expectation value of the twist operator along the y direction defined below corresponds to the many-body Chern number C:

$$T_y = \exp\left(i\frac{2\pi}{L}\sum_j y_j n_{jc}\right) \tag{10}$$

Here, y_j is the y-coordinate of site j, and n_{jc} is the number operator for the conduction electrons at site j. Although the twist operator is an exponential operator containing the electron-number operator, it is diagonal with respect to real-space configurations and can therefore be measured easily in VMC.

Figure 2 shows the flux dependence of the argument for the triple-Q insulator and for a nonmagnetic Kondo insulator on the square lattice at half filling. For the Kondo insulator, the argument does not change with the flux, indicating that it is topologically trivial. In contrast, for the triple-Q insulator the argument increases linearly with the flux, which indicates that it is indeed a topologically nontrivial many-body Chern insulator with $C = 1$.

B. Kitaev-Kondo model

Next, we present results on the Kitaev-Kondo model, where the Kitaev model on the honeycomb lattice is coupled to a conduction-electron layer via the Kondo coupling [84–87]. The Kitaev model is a system whose ground state is a topological quantum spin liquid, the Kitaev spin liquid, in which Majorana fermions relevant to topological quantum computation

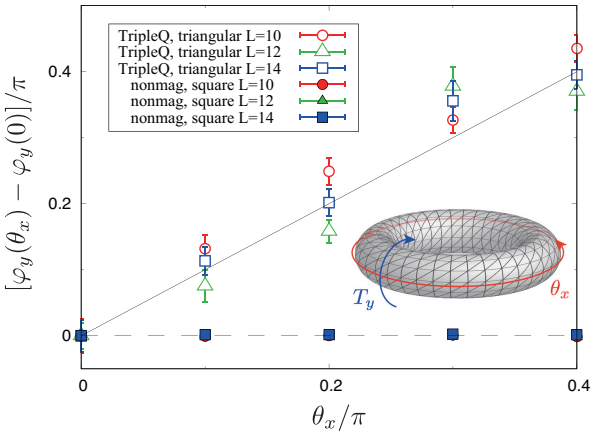

FIG. 2. Flux dependence of the argument of the expectation value of the twist operator. Open and filled symbols represent the results for the triple-Q insulator on the triangular lattice at quarter filling and the Kondo insulator on the square lattice at half filling, respectively. Shapes of the symbols represent different system sizes. Black lines are guides to the eye. Inset shows a schematic picture of the flux insertion θ_x and the twist operator T_y. Adapted from Ref. [51] with modifications for the present report.

emerge [88]. Its Hamiltonian is defined as follows:

$$\mathcal{H}_{\text{Kitaev}} = K \sum_{\gamma=x,y,z} \sum_{\langle i,j\rangle_\gamma} S_i^\gamma S_j^\gamma \qquad (11)$$

Here, S_i^γ is the γ component of the spin operator at site i, and $\langle i,j\rangle_\gamma$ indicates that sites i and j are on a γ bond. K denotes the strength of the Kitaev interaction.

Although the Kitaev model is a many-body problem when viewed in terms of the spin degrees of freedom, it is known to be exactly solvable by expressing the spin degrees of freedom in an alternative representation and exploiting the existence of conserved quantities such as the flux operator, as explained later. For instance, in Kitaev's original paper, a spin with a two-dimensional local Hilbert space is represented by four Majorana fermions [88]. Although the introduction of Majorana fermions enlarges the Hilbert space beyond the original one, it was shown that the true ground state can be expressed as the ground state of the free Majorana fermions with a projection onto the original Hilbert space. The model can also be solved using a representation based on the Jordan-Wigner transformation [89, 90].

In fact, it has been pointed out that the Abrikosov fermion representation introduced in the previous section and the Kitaev Majorana representation can be connected by a simple transformation matrix [91–94]. Using this, one can construct a Gutzwiller-projected wavefunction in the Abrikosov fermion representation corresponding to the exact Kitaev spin liquid state because the Gutzwiller factor used in VMC projects onto the physical Hilbert space.

Building on this, we use VMC to analyze the Kitaev-Kondo model on the honeycomb lattice at half filling, namely the model in which the conduction layer and the Kitaev model as the localized spin layer are coupled through the Kondo coupling,

$$\mathcal{H}_{\text{Kitaev-Kondo}} = \mathcal{H}_{\text{Kondo}} + \mathcal{H}_{\text{Kitaev}}. \qquad (12)$$

To clarify physical properties of the Kitaev-Kondo model, we measure the magnetic order parameter and the site-averaged on-site Kondo-singlet correlation $\langle \boldsymbol{S}_{\text{c}} \cdot \boldsymbol{S}_{\text{s}} \rangle$, which are typical physical quantities characterizing the ground state of the Kondo lattice model. We also compute the expectation value of the flux operator defined on each hexagonal plaquette of the honeycomb lattice, $W_p = \prod_{i\in p} 2S_i^{\gamma_i}$, where the subscripts of S represent the six sites around the hexagonal plaquette and γ_i denotes the bond type of the link at site i that points outside the plaquette p. This is a conserved quantity in the Kitaev model, and $\langle W_p \rangle = 1$ in the Kitaev spin liquid.

We first analyze the honeycomb Kondo lattice model with the Kitaev interaction set to zero, as shown in Fig. 3. As J/t is increased, the magnetic moment of the conduction electrons $|\boldsymbol{S}_{\text{c}}|$ forms while that of the localized spins $|\boldsymbol{S}_{\text{s}}|$ decreases. This behavior is attributed to the magnetically ordered state generated by the RKKY interaction and the

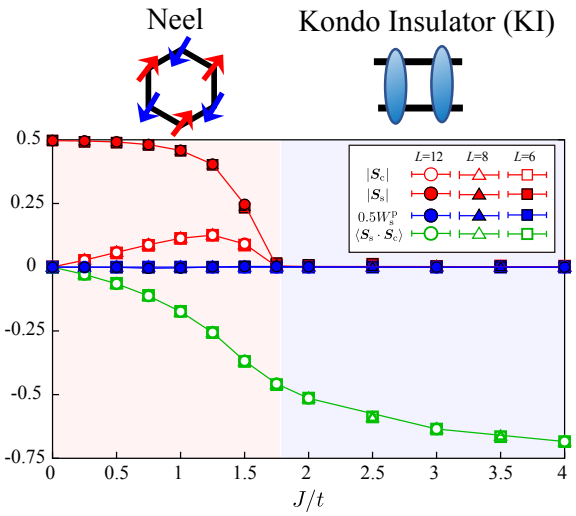

FIG. 3. J dependence of physical quantities for the honeycomb Kondo lattice model. Red open and filled symbols represent the magnetic order parameters of the conduction electrons and the localized spins, respectively. Blue filled symbols represent the expectation values of the flux operator on the localized spin layer. Green open symbols represent the Kondo-singlet correlation. Shapes of the symbols represent different system sizes. Schematic pictures of the Néel state and the Kondo insulator (KI) are shown on top of the figure. Thin lines and shaded areas are guides to the eye.

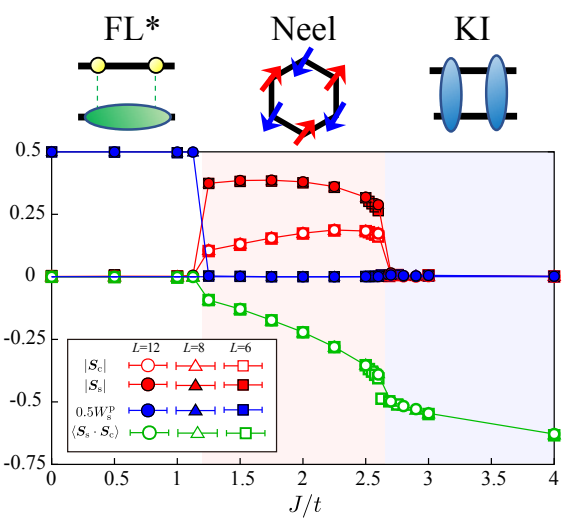

FIG. 4. J dependence of various physical quantities for the Kitaev-Kondo model for $K/t = 4$. Schematic pictures of the fractionalized Fermi liquid (FL*) state, the Néel state, and the Kondo insulator (KI) are shown on top of the figure. Notations are the same as in Fig. 3.

reduction of $|\boldsymbol{S}_{\rm s}|$ due to Kondo screening. Because the RKKY interaction on the honeycomb lattice produces an antiferromagnetic effective spin interaction, the spin configuration is of Néel type [95]. As J/t is increased further, not only the localized-spin order but also the conduction-electron spin order is suppressed, and the system undergoes a continuous transition to a nonmagnetic Kondo insulator around $J/t \sim 1.75$. This is qualitatively consistent with the results of the same model analyzed by the quantum Monte Carlo method [96].

Figure 4 shows the J dependence of various physical quantities at $K/t = 4$. For $J/t < 1.2$, both the magnetic order parameter and the Kondo-singlet correlation are numerically nearly zero, and the expectation value of the flux operator, plotted as the blue filled symbols and characteristic of the Kitaev spin liquid, takes $\langle W_p \rangle = 1$. This result suggests that the conduction layer and the Kitaev layer are decoupled, which is interpreted as a fractionalized Fermi liquid (FL*), as pointed out in previous studies using mean-field theory [84, 85]. As J/t is increased, the Kondo-singlet correlation eventually forms and $\langle W_p \rangle$ drops to nearly zero. For $1.2 < J/t < 2.7$, the magnetic order parameter, plotted as the red open and filled symbols, remains finite. As in the $K/t = 0$ result, the antiferromagnetic state with a Néel pattern is realized, which is naturally interpreted as a result of the RKKY interaction. Increasing J/t further suppresses the spin order through Kondo screening, and the system transitions into a nonmagnetic Kondo insulator. An interesting point is that the transition between the magnetic phase and the Kondo insulator is first-order-like. Since the Kondo lattice model exhibits a continuous transition, this suggests the existence of a quantum tricritical point in the K-J phase diagram.

IV. SUMMARY

In summary, we have presented two analyses of topological magnetic states performed with the variational Monte Carlo method. In the first part, we investigate the stability of the magnetic topological insulator in the Kondo lattice model on the triangular lattice and propose the efficient approach to compute the many-body Chern number in VMC. In the second part, we report the VMC analysis of the ground state in the Kitaev-Kondo model on the honeycomb lattice.

In the study on the magnetic topological insulator, we compute the many-body Chern number from the expectation value of the twist operator, which is well suited to VMC measurements. As in the present case, the twist operator can be applied to the measurement of other topological numbers in addition to the many-body Chern number. For example, in Ref. [97], VMC measurement of the twist operator is used to compute the many-body Zak phase. We have recently implemented the twist operator measurement functionality in mVMC [41, 98], open-source software developed under the Project for advancement of software usability in materials science (PASUMS) [99]. Since the twist operator has also attracted attention as a quantity capable of detecting other topological phase transitions [100–102], such applications of twist operator measurement to topological states are expected to further promote the use of mVMC.

As shown in the second study, VMC can analyze topological quantum spin liquids together with many-body effects of charge degrees of freedom. How topological properties are affected by the inclusion of charge degrees of freedom, and whether new exotic states emerge, are research directions to pursue as future work.

ACKNOWLEDGMENTS

We acknowledge Takahiro Misawa for collaboration on these studies. We also thank the Supercomputer Center, the Institute for Solid State Physics, the University of Tokyo and the Information Technology Center, the University of Tokyo for their facilities. This work was supported by Grant-in-Aid for Scientific Research (Nos. JP16H06345, JP19K03739, JP19K14645, JP23H03818, and JP23K13055) from Ministry of Education, Culture, Sports, Science and Technology, Japan.

[1] M. Imada, A. Fujimori, and Y. Tokura, Rev. Mod. Phys. **70**, 1039 (1998).
[2] B. Keimer, S. A. Kivelson, M. R. Norman, S. Uchida, and J. Zaanen, Nature **518**, 179 (2015).
[3] G. Stewart, Rev. Mod. Phys. **83**, 1589 (2011).
[4] H. Hosono and K. Kuroki, Physica C **514**, 399 (2015).
[5] Q. Si, R. Yu, and E. Abrahams, Nat. Rev. Mater. **1**, 16017 (2016).
[6] Y. Nomura and R. Arita, Rep. Prog. Phys. **85**, 052501 (2022).
[7] P. Puphal, T. Schäfer, B. Keimer, and M. Hepting, Nat. Rev. Phys. **8**, 70 (2026).
[8] S. Paschen and Q. Si, Nat. Rev. Phys. **3**, 9 (2021).
[9] L. Balents, Nature **464**, 199 (2010).
[10] C. Broholm, R. J. Cava, S. Kivelson, D. Nocera, M. Norman, and T. Senthil, Science **367**, eaay0668 (2020).
[11] H. Takagi, T. Takayama, G. Jackeli, G. Khaliullin, and S. E. Nagler, Nat. Rev. Phys. **1**, 264 (2019).
[12] S. Trebst and C. Hickey, Phys. Rep. **950**, 1 (2022).
[13] N. Nagaosa, J. Sinova, S. Onoda, A. H. MacDonald, and N. P. Ong, Rev. Mod. Phys. **82**, 1539 (2010).
[14] M. Z. Hasan and C. L. Kane, Rev. Mod. Phys. **82**, 3045 (2010).
[15] Y. Tokura, K. Yasuda, and A. Tsukazaki, Nat. Rev. Phys. **1**, 126 (2019).

[16] C.-X. Liu, S.-C. Zhang, and X.-L. Qi, Annu. Rev. Condens. Matter Phys. **7**, 301 (2016).
[17] B. A. Bernevig, C. Felser, and H. Beidenkopf, Nature **603**, 41 (2022).
[18] F. Becca and S. Sorella, *Quantum Monte Carlo approaches for correlated systems* (Cambridge University Press, 2017).
[19] W. L. McMillan, Phys. Rev. **138**, A442 (1965).
[20] D. Ceperley, G. V. Chester, and M. H. Kalos, Phys. Rev. B **16**, 3081 (1977).
[21] C. Gros, R. Joynt, and T. M. Rice, Phys. Rev. B **36**, 381 (1987).
[22] H. Yokoyama and H. Shiba, J. Phys. Soc. Jpn. **56**, 1490 (1987).
[23] T. Giamarchi and C. Lhuillier, Phys. Rev. B **43**, 12943 (1991).
[24] G. Carleo, F. Becca, M. Schiró, and M. Fabrizio, Sci. Rep. **2**, 243 (2012).
[25] G. Carleo, F. Becca, L. Sanchez-Palencia, S. Sorella, and M. Fabrizio, Phys. Rev. A **89**, 031602 (2014).
[26] L. Cevolani, G. Carleo, and L. Sanchez-Palencia, Phys. Rev. A **92**, 041603 (2015).
[27] K. Ido, T. Ohgoe, and M. Imada, Phys. Rev. B **92**, 245106 (2015).
[28] K. Takai, K. Ido, T. Misawa, Y. Yamaji, and M. Imada, J. Phys. Soc. Jpn. **85**, 034601 (2016).
[29] Y. Nomura, N. Yoshioka, and F. Nori, Phys. Rev. Lett. **127**, 060601 (2021).
[30] N. Yoshioka and R. Hamazaki, Phys. Rev. B **99**, 214306 (2019).
[31] A. Nagy and V. Savona, Phys. Rev. Lett. **122**, 250501 (2019).
[32] M. J. Hartmann and G. Carleo, Phys. Rev. Lett. **122**, 250502 (2019).
[33] F. Vicentini, A. Biella, N. Regnault, and C. Ciuti, Phys. Rev. Lett. **122**, 250503 (2019).
[34] T. Li and F. Yang, Phys. Rev. B **81**, 214509 (2010).
[35] K. Ido, T. Ohgoe, and M. Imada, Sci. Adv. **3**, e1700718 (2017).
[36] K. Ido, M. Imada, and T. Misawa, Phys. Rev. B **101**, 075124 (2020).
[37] M. Charlebois and M. Imada, Phys. Rev. X **10**, 041023 (2020).
[38] A. Mahajan, P. J. Robinson, J. Lee, and D. R. Reichman, Phys. Rev. B **112**, 184310 (2025).
[39] D. Tahara and M. Imada, J. Phys. Soc. Jpn. **77**, 114701 (2008).
[40] M. Kurita, Y. Yamaji, S. Morita, and M. Imada, Phys. Rev. B **92**, 035122 (2015).
[41] T. Misawa, S. Morita, K. Yoshimi, M. Kawamura, Y. Motoyama, K. Ido, T. Ohgoe, M. Imada, and T. Kato, Comput. Phys. Commun. **235**, 447 (2019).
[42] H.-H. Zhao, K. Ido, S. Morita, and M. Imada, Phys. Rev. B **96**, 085103 (2017).
[43] Y. Nomura, A. S. Darmawan, Y. Yamaji, and M. Imada, Phys. Rev. B **96**, 205152 (2017).
[44] T. Ohgoe, M. Hirayama, T. Misawa, K. Ido, Y. Yamaji, and M. Imada, Phys. Rev. B **101**, 045124 (2020).
[45] M. T. Schmid, J.-B. Morée, R. Kaneko, Y. Yamaji, and M. Imada, Phys. Rev. X **13**, 041036 (2023).
[46] T. Misawa, K. Nakamura, and M. Imada, J. Phys. Soc. Jpn. **80**, 023704 (2011).
[47] T. Misawa, K. Nakamura, and M. Imada, Phys. Rev. Lett. **108**, 177007 (2012).
[48] T. Misawa and M. Imada, Nat. Commun. **5**, 5738 (2014).
[49] K. Ido, K. Yoshimi, T. Misawa, and M. Imada, npj Quantum Mater. **7**, 48 (2022).
[50] K. Yoshimi, T. Misawa, T. Tsumuraya, and H. Seo, Phys. Rev. Lett. **131**, 036401 (2023).
[51] K. Ido and T. Misawa, Phys. Rev. B **109**, 245114 (2024).
[52] N. Metropolis, A. W. Rosenbluth, M. N. Rosenbluth, A. H. Teller, and E. Teller, J. Chem. Phys. **21**, 1087 (1953).
[53] W. K. Hastings, Biometrika **57**, 97 (1970).
[54] S. Sorella, Phys. Rev. B **64**, 024512 (2001).
[55] S.-I. Amari, Neural Comput. **10**, 251 (1998).
[56] M. C. Gutzwiller, Phys. Rev. Lett. **10**, 159 (1963).
[57] R. Jastrow, Phys. Rev. **98**, 1479 (1955).
[58] A. A. Abrikosov, Physics Physique Fizika **2**, 5 (1965).
[59] J. Kondo, Prog. Theor. Phys. **32**, 37 (1964).
[60] M. A. Ruderman and C. Kittel, Phys. Rev. **96**, 99 (1954).
[61] T. Kasuya, Prog. Theor. Phys. **16**, 45 (1956).
[62] K. Yosida, Phys. Rev. **106**, 893 (1957).
[63] S. Doniach, Physica B+C **91**, 231 (1977).
[64] Y. Motome, K. Nakamikawa, Y. Yamaji, and M. Udagawa, Phys. Rev. Lett. **105**, 036403 (2010).

[65] J. Otsuki, H. Kusunose, and Y. Kuramoto, J. Phys. Soc. Jpn. **78**, 034719 (2009).
[66] R. Peters, S. Hoshino, N. Kawakami, J. Otsuki, and Y. Kuramoto, Phys. Rev. B **87**, 165133 (2013).
[67] T. Misawa, J. Yoshitake, and Y. Motome, Phys. Rev. Lett. **110**, 246401 (2013).
[68] H. Tsunetsugu, M. Sigrist, and K. Ueda, Rev. Mod. Phys. **69**, 809 (1997).
[69] G. R. Stewart, Rev. Mod. Phys. **73**, 797 (2001).
[70] H. v. Löhneysen, A. Rosch, M. Vojta, and P. Wölfle, Rev. Mod. Phys. **79**, 1015 (2007).
[71] P. Gegenwart, Q. Si, and F. Steglich, Nat. Phys. **4**, 186 (2008).
[72] Q. Si and F. Steglich, Science **329**, 1161 (2010).
[73] K. Ohgushi, S. Murakami, and N. Nagaosa, Phys. Rev. B **62**, R6065 (2000).
[74] I. Martin and C. D. Batista, Phys. Rev. Lett. **101**, 156402 (2008).
[75] S. Kumar and J. van den Brink, Phys. Rev. Lett. **105**, 216405 (2010).
[76] Y. Akagi and Y. Motome, J. Phys. Soc. Jpn. **79**, 083711 (2010).
[77] Y. Akagi, M. Udagawa, and Y. Motome, Phys. Rev. Lett. **108**, 096401 (2012).
[78] Y. Akagi, M. Udagawa, and Y. Motome, J. Phys. Soc. Jpn. **82**, 123709 (2013).
[79] R. Takagi, J. S. White, S. Hayami, R. Arita, D. Honecker, H. M. Rønnow, Y. Tokura, and S. Seki, Sci. Adv. **4**, eaau3402 (2018).
[80] P. Park, W. Cho, C. Kim, Y. An, Y.-G. Kang, M. Avdeev, R. Sibille, K. Iida, R. Kajimoto, K. H. Lee, *et al.*, Nat. Commun. **14**, 8346 (2023).
[81] H. Takagi, R. Takagi, S. Minami, T. Nomoto, K. Ohishi, M.-T. Suzuki, Y. Yanagi, M. Hirayama, N. Khanh, K. Karube, *et al.*, Nat. Phys. **19**, 961 (2023).
[82] R. Resta, Phys. Rev. Lett. **80**, 1800 (1998).
[83] H. Dehghani, Z.-P. Cian, M. Hafezi, and M. Barkeshli, Phys. Rev. B **103**, 075102 (2021).
[84] U. F. Seifert, T. Meng, and M. Vojta, Phys. Rev. B **97**, 085118 (2018).
[85] W. Choi, P. W. Klein, A. Rosch, and Y. B. Kim, Phys. Rev. B **98**, 155123 (2018).
[86] V. S. de Carvalho, R. M. Teixeira, H. Freire, and E. Miranda, Phys. Rev. B **103**, 174512 (2021).
[87] A. M. Tsvelik and P. Coleman, Phys. Rev. B **106**, 125144 (2022).
[88] A. Kitaev, Annals of Physics **321**, 2 (2006), january Special Issue.
[89] X.-Y. Feng, G.-M. Zhang, and T. Xiang, Phys. Rev. Lett. **98**, 087204 (2007).
[90] H.-D. Chen and Z. Nussinov, J. Phys. A **41**, 075001 (2008).
[91] F. J. Burnell and C. Nayak, Phys. Rev. B **84**, 125125 (2011).
[92] R. Schaffer, S. Bhattacharjee, and Y. B. Kim, Phys. Rev. B **86**, 224417 (2012).
[93] J. Fu, J. Knolle, and N. B. Perkins, Phys. Rev. B **97**, 115142 (2018).
[94] M. Udagawa, J. Phys. Condens. Matter. **33**, 254001 (2021).
[95] M. Sherafati and S. Satpathy, Phys. Rev. B **83**, 165425 (2011).
[96] M. Raczkowski, B. Danu, and F. F. Assaad, Phys. Rev. B **106**, L161115 (2022).
[97] T. Misawa and M. Naka, Phys. Rev. B **108**, L081120 (2023).
[98] https://www.pasums.issp.u-tokyo.ac.jp/mvmc/en/.
[99] https://www.pasums.issp.u-tokyo.ac.jp/en/.
[100] M. Oshikawa, Phys. Rev. Lett. **84**, 3370 (2000).
[101] M. Nakamura and J. Voit, Phys. Rev. B **65**, 153110 (2002).
[102] M. Nakamura and S. Todo, Phys. Rev. Lett. **89**, 077204 (2002).